photonics

MDPI

Article

Effect of Dual-Pulse Temporal Shaping on Ultraviolet Nanosecond Laser Damage of Fused Silica Surface in High Fluence Regime

Wenfeng Liu [1,2], Mingying Sun [1,*], Yajing Guo [1], Yiqun Shi [1,2], Yingming Xu [1,2], Zhaoyang Jiao [1], Zijian Cui [1] and Jianqiang Zhu [1]

[1] National Laboratory on High Power Laser and Physics, Shanghai Institute of Optics and Fine Mechanics, Chinese Academy of Sciences, Shanghai 201800, China
[2] Center of Materials Science and Optoelectronics Engineering, University of Chinese Academy of Sciences, Beijing 100049, China
* Correspondence: sunmy@siom.ac.cn

Abstract: We present the effect of dual-pulse temporal shaping on the ultraviolet nanosecond laser damage characteristics of a fused silica exit surface in a high fluence regime. The pre- and post-pulse have the opposite effects on the damage behavior at a pulse delay of 20 ns. The pre-pulse irradiation significantly increases the main-pulse threshold, making it much higher than that of the single-pulse threshold, while the post-pulse has little effect on the main-pulse threshold. For near-threshold damage sites, the pre-pulse reduces the average damage size and depth, making them smaller than those of the single-pulse, while the post-pulse drastically increases the average size and depth, making them much larger than those of the single-pulse. The average size of the damage site is monotonously increased from 43.6 μm to 127.9 μm with increasing post-pulse energy. For the pre-pulse with a shape factor of 0.61, the damage threshold of the main pulse increases with increasing delay and nearly stabilizes after 10 ns. The underlying mechanism of the temporal-shaping effect on laser damage is discussed based on the applied precursor modification to absorption enhancement, which could provide insights for studying ultraviolet laser damage of fused silica optics.

Keywords: temporal shaping; damage in high fluence regime; ultraviolet nanosecond laser; fused silica

Citation: Liu, W.; Sun, M.; Guo, Y.; Shi, Y.; Xu, Y.; Jiao, Z.; Cui, Z.; Zhu, J. Effect of Dual-Pulse Temporal Shaping on Ultraviolet Nanosecond Laser Damage of Fused Silica Surface in High Fluence Regime. *Photonics* **2022**, *9*, 834. https://doi.org/10.3390/photonics9110834

Received: 13 October 2022
Accepted: 3 November 2022
Published: 6 November 2022

1. Introduction

Ultraviolet (UV) laser-induced damage of fused silica optics is of great concern in nanosecond high-power laser systems for inertial confinement fusion, because the growth of surface damage sites severely limits the lifetime of large aperture optics [1,2]. Most of the precursors causing laser damage to optics under low fluence conditions (<20 J/cm^2) are related to fractures, scratches and impurities associated with the polished layer, which can be efficiently removed by acid leaching [3–6]. However, the damage performance of the surface of optics under a high fluence regime (>20 J/cm^2) is also important, since surface flaws or features on the upstream optics can lead to strong modulation of laser beams in the downstream optics, resulting in higher local fluence on the optical surfaces [7]. These hot spots with high local fluence are likely to initiate uncontrolled damage, reducing the lifetime of the optical materials. High-fluence damage precursors are substantially smaller than one micron [8] and, therefore, are not readily observable prior to the onset of damage. As such, they are known as "invisible" precursors [9]. Therefore, it would be very useful to explore the damage dynamics initialized by high-fluence damage precursors for high power laser systems.

High-fluence laser damage has already attracted attention. Laser pulses with high fluence and high intensity have the ability to excite high-fluence precursors to deposit laser energy and thus produce damage. The morphology and microstructure of laser damage

have been investigated to construct a physical model of the damage crater and to gain critical insights into laser damage physics [10]. Damage precursors in high-quality silica surfaces lead to a large increase in the damage density near 20–30 J/cm^2 but a gentle increase beyond this fluence level. A close connection was established between the small-beam damage test results of damage probability versus fluence and the large-beam damage test results of damage density versus fluence [7]. Past research has presented the dependences of the damage threshold and density on high fluence and the method of reducing the precursor density from a processing perspective [8]. However, novel methods from a laser perspective can provide unique ways to further understand the damage mechanism in high fluence regimes and even to precisely modify precursors and control damage dynamics.

The temporal shape of a laser pulse has a great impact on the damage initiation and morphology, because laser damage is closely related to the intensity and fluence of the laser pulse, which are connected by temporal distribution [11–14]. First, by using a laser pulse with various temporal shapes, it was demonstrated that the majority of energy deposited during laser-induced damage on the exit surface of SiO_2 occurs during a laser-driven absorption front, which explains the dependence of the damage spot size on the pulse width [15]. Second, by producing damage with singe pulse of various widths and dual-pulse train of various delays, it has been demonstrated that the properties of any hypothetical thermal absorber become highly constrained. By analyzing the dependence of the damage density on the pulse width and pulse delay of a dual pulse, it was shown that the density of damage was determined by the laser intensity, rather than its fluence [16]. Third, pump and probe damage testing was performed to investigate the transient material modifications associated with laser damage in optical materials [17]. The initial energy deposition and resulting plasma modify the surrounding material to become absorbing and longer lived in fused silica (decaying over ~100 μs). The mechanisms for additional energy deposition by a probe pulse in the material may be different in the various stages of transient material modifications, leading to a damage site. Forth, by pulse width optimization or temporal-shaping, the pre-exposure of the laser pulse with a fluence lower than the threshold can effectively inhibit the damage of subsequent laser pulses, i.e., the conditioning effect [18,19]. Gaussian pulses that are temporally truncated at the peak intensity have a higher N-on-1 threshold than a normal Gaussian pulse. The falling edge of the Gaussian pulse will increase the energy absorbed in the surrounding host material, leading to a lower threshold [19]. Therefore, pulse shaping has been proved to be a valuable tool to study the damage mechanism and control damage dynamics, including suppressing or aggravating laser damage.

The dual-pulse train is a special pulse-shaping method that has been widely applied to study ultrashort and short pulse damage and ablation [15–17,20–24]. It can provide flexible modulations of the pulse-train shapes by adjusting the energy ratio and temporal delay at the same time. In this paper, therefore, we propose a temporally shaped, dual-pulse train in the nanosecond scale to investigate the exit surface damage dynamics of fused silica induced in the UV high-fluence regime. First, we continuously change the temporal shapes of dual-pulse train by adjusting their energy ratio at a delay of 20 ns to study the impact of the pre- or post-pulse on laser damage characteristics, including the damage threshold, size and depth. A detailed comparative analysis of the experimental results demonstrates that the pre-pulse results in a higher main-pulse threshold and smaller damage size, while the post-pulse significantly increases the damage size. Second, we adjust the temporal delay of the ramp-up-shaped dual pulses to show the temporal relaxation of the pre-pulse's influence on the damage threshold of the main-pulse. Finally, we discuss the underlying mechanisms of the damage modulation by the temporal-shaping the dual-pulse train.

2. Experimental Setup and Methods

The damage testing setup with UV temporally shaped, double-nanosecond-pulse train is shown in Figure 1; it comprises a laser source, frequency conversion, beam expander, energy adjustment, dual-pulse train generation, laser diagnostics and sample stages. The

nanosecond laser source delivers pulses at 1064 nm with a beam diameter of 7 mm and a repetition rate of 10 Hz. Two pieces of BBO crystals are used as the frequency conversion module to obtain a 355 nm laser pulse with a FWHM width of 7 ns. The beam expander module, which consists of concave and convex lenses, is used to reduce the divergence of the laser beams to ensure the same size of the focal spot of the two sub-pulses with paths of different lengths. The combination of the half wave-plate (HWP) and polarizer is used to adjust the total energy of the dual-pulse. The dual-pulse train generation module consists of pulse splitting, delay line and combination. HWP and a polarization beam splitter (PBS) are used to generate two sub-pulses with different polarizations and to control their energy ratio by rotating the HWP. In the delay line, the path of a long delay, i.e., up to tens of nanoseconds, is generated with multiple reflections between small-angle mirrors. The second PBS combines the two sub-pulses with different delays to obtain the dual-pulse train with the orthogonal polarizations. The dual-pulse train is focused on the sample exit surface with a small incident angle. The focal spot and pulse energy are monitored by the beam analyzer and energy meter in the sampling optical path, respectively. Beam paths of the two sub-pulses are strictly aligned by the beam analyzer to make them spatially overlapped at the focus. In order to explore the damage performance at high fluence, it is necessary to carry out a laser damage threshold test with beams sizes much smaller than those typically applied in the Laser-Induced Damage Threshold (LIDT) tests [7]. Therefore, we chose a focal length of the target lens of 300 mm, and thus, the $1/e^2$ diameter of the focal spot is 67 μm.

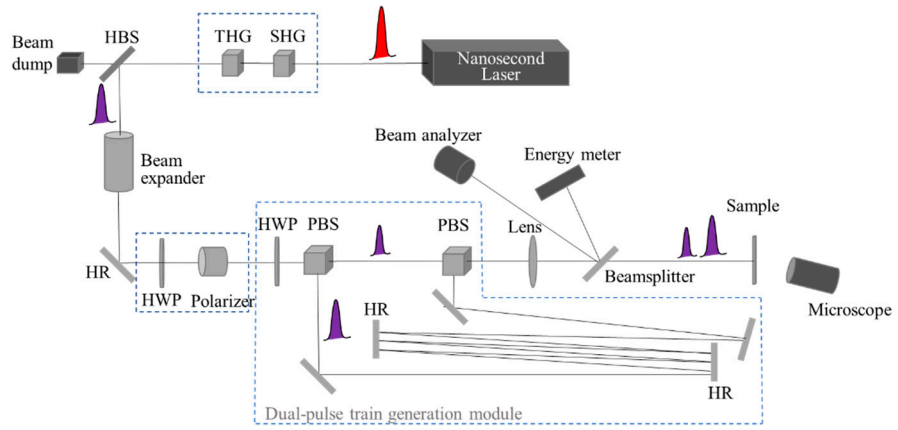

Figure 1. Schematic of nanosecond dual-pulse laser damage test setup. SHG: second harmonic generation crystal; THG: third harmonic generation crystal; HBS: harmonic beam splitters; HR: high reflectance mirror; HWP: half wave-plate; PBS: polarization beam splitter.

Fused silica samples (50 mm × 50 mm with 2.4 mm thick) were prepared with surface finishing and polishing processes including hydrofluoric acid etching to reduce surface and subsurface defects, thereby improving the surface damage threshold [2]. The surface roughness was about 0.8 nm. All samples were ultrasonic cleaning in absolute alcohol before being placed in an ultra-clean room for drying to clean the surface of contaminants. The one-on-one damage threshold tests were carried out in air; 15 sites were irradiated for each fluence, and the test fluences with at least 10 steps were selected to cover the damage probability of 0~100%. We repeated the measurement with the same parameters using different fused silica samples. Damage sites on the exit surface were initially determined by in-line microscopy and then characterized off-line in detail by high-magnification digital microscopy (HIROX KH-8700). We then plotted the fraction of sites that were damaged as a function of the beam fluence. By fitting the damage probability curve with the fluence, we obtained dual-pulse train thresholds for 0% and 100% damage probability. However, the damage threshold in this work denotes the threshold for 0% probability without specifications.

As shown in Figure 2, the two sub-pulses are named the main-pulse, with larger energy, and the pre-pulse (or post-pulse), with less energy. The pulse energy for the two sub-pulses is independently adjusted and their fluences are expressed as ϕ_{main} and ϕ_p, respectively. Then, the dual-pulse train fluence can be denoted as $\phi_{train} = \phi_p + \phi_{main}$. The dual-pulse train shape is indicated by the shape factor $\eta = \pm\phi_p/\phi_{main}$, i.e., the fluence ratio of the pre-/post-pulse to the main pulse, while the sign indicates the pre- and post-pulse cases, respectively. For the pre-pulse case, $\eta > 0$, the dual-pulse has a ramp-up shape, as shown in Figure 2a; here, ϕ_p denotes the pre-pulse fluence. For the post-pulse, $\eta < 0$ and the dual–pulse has a ramp-down shape as shown in Figure 2b; here, ϕ_p denotes the post-pulse fluence. As a special case, $\eta = 0$ denotes the case of a single pulse.

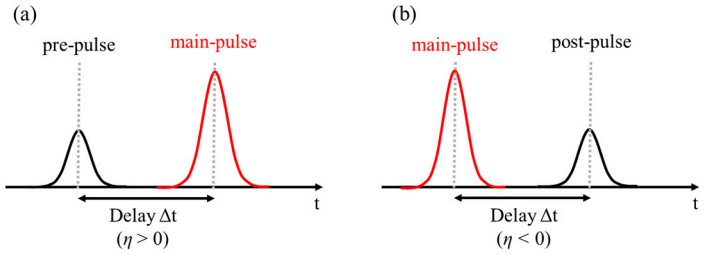

Figure 2. Schematic diagram of nanosecond dual-pulse temporal shaping. (**a**) Ramp-up shape with pre-pulse and main-pulse; (**b**) Ramp-down shape with main-pulse and post-pulse.

In the laser damage experiment, we carried out laser damage threshold tests with the dual-pulse train with various shape factors and pulse delays. Each test was done for the dual-pulse train with the fixed shape factor and pulse delay. In detail, in each test, the dual-pulse train is regarded as one pulse and the overall laser energy is adjusted, so each site is irradiated by a dual-pulse train with the same shape factor η. Therefore, we can directly obtain the damage threshold F_{train} of the dual-pulse using the one-on-one test method. The corresponding fluence for the main-pulse F_{main} and the pre-pulse or post-pulse F_p are calculated with the formula of η and the measured F_{train}. In addition, the single pulse threshold for the case of $\eta = 0$ was also measured and is denoted as F_{single}.

The temporal delay between the two sub-pulses in the experiment can be adjusted continuously from 0 ns to 50 ns, and the accuracy of the pulse delay is dependent on the linear stages <0.5 mm (1.67 ps). Since the sub-pulse width is 7 ns, we chose a pulse delay of 20 ns to investigate the influence of pulse shape on the damage behavior for two reasons. First, for the ramp-up shaped train, a delay of 20 ns leads to a 100% threshold, as experimentally revealed in this work. Second, for the ramp-down shaped train, once the main pulse induces the onset of the damage site, and no particle ejection in the damaged zone happens until the delay is larger than 25 ns [25], so a delay of 20 ns could lead to the highest absorptivity of the post-pulse energy.

3. Experimental Results and Analysis

3.1. Effect of Temporal Shaping on Damage Threshold

We carried out the damage threshold test with a dual-pulse train and a delay of 20 ns and investigated the impact of dual-pulse shapes on the laser damage threshold. The experimental results of damage probability with laser fluence of pulse trains for various shape factors η are shown in Figure 3a. Based on the fitting lines, we obtained the 0% probability damage threshold of the dual-pulse train F_{train} with various shapes, as shown in Figure 3b by the circles. Then, we calculated the main-pulse threshold F_{main} based on the definition of η, also shown in Figure 3b by the squares. We change the shape factor η in the experiment such that the train shape first ramps down ($\eta < 0$) and then ramps up ($\eta > 0$), as shown in the insets of Figure 3b.

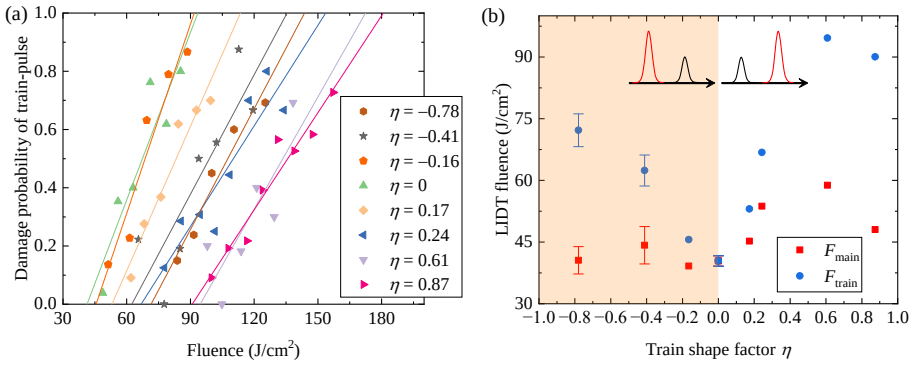

Figure 3. (**a**) Relations between damage probability and laser fluence of pulse trains with different shape factors η at the 20 ns delay. (**b**) Dependence of dual-pulse train threshold F_{train} and main-pulse threshold F_{main} on the factor η at the 20 ns delay. Inset: Sketches of temporal shapes of dual-pulse train.

For $\eta < 0$, the dual-pulse train has a ramp-down shape. By increasing the shape factor η from -0.78 to 0, the train threshold F_{train} decreases, but the main-pulse threshold F_{main} is almost invariable and keeps the same to single-pulse threshold F_{single}, which is ~40.4 J/cm^2. It indicates that the post-pulse has little influence on the damage initiation and main-pulse damage threshold while the main pulse is responsible for the initiation of the damage site.

For $\eta > 0$, the dual-pulse train has a ramp-up shape. By increasing the shape factor η from 0 to 0.87, both of the train threshold F_{train} and the main-pulse threshold F_{main} increase gradually with the similar trends. Now we focus on the effect of the pre-pulse on the main-pulse threshold. When $\eta = 0.61$, F_{main} reaches the maximum of 58.8 J/cm^2, which is higher by 45.5% than single-pulse threshold F_{single}. The results show that the pre-pulse has a great impact on the damage initiation and significantly increases the main-pulse damage threshold. It indicates that the pre-pulse has a positive modification of the damage precursors to make them less absorptive to laser energy of the subsequent main pulse, which is similar to the conditioning effect.

By comparing the results with $\eta < 0$ and $\eta > 0$, we can find that the effect of the train shaping on the main-pulse threshold F_{main} is asymmetrical about $\eta = 0$. The threshold for the ramp-up shape ($\eta > 0$) is significantly higher than that for the ramp-down shape ($\eta < 0$), although they have the similar train widths (FWHM). Especially, the pre-pulse at the case of $\eta = 0.61$ results in a great enhancement in main-pulse threshold. Therefore, it is qualitatively consistent to the enhancement of N-on-1 threshold by pulse shaping of the 3 ns Gaussian pulse reported in [19]. For temporal-shaped dual-pulse, we can conclude that pre-pulse and post-pulse play different roles in the damage initiation. The pre-pulse with a suitable fluence can obviously increase the main-pulse threshold by positively modifying the damage precursors, while the post-pulse has little contributions to the damage initiation.

3.2. Effect of Temporal Shaping on Damage Morphology

Since the temporal shaping of the dual-pulse has great effects on the damage threshold as shown in Figure 3b, there should be some corresponding responses in damage morphology. Therefore, the influence of pulse-train shapes on the damage morphology is further explored to analyze the modulation roles of the pre-pulse or post-pulse on the damage dynamics. A typical microscopic morphology of UV nanosecond-laser-induced damage site of fused silica exit surface is shown in Figure 4, where it has a molten core region, surrounded by a near concentric region of fractured material. The core region forms in the initial damage process, and most of the material has been ejected from the fused core. The thermal explosion is evident in the ring-shaped damage region, indicating that mechanical damage is accompanied by lamellar fracture of the material. In order to quantitatively analyze the modulation mechanism of temporal-shaping on the surface damage, as demonstrated in Figure 4, we measured the diameter of the core region as well as that of the outer region of all the damage sites obtained in the laser damage threshold test.

Thus all of these damage sites are induced by near-threshold fluences. The representative damage morphologies for various shapes are shown in Figure 5 and the detailed analysis of the damage diameters on laser fluence and shape factors are presented in Figures 6–9.

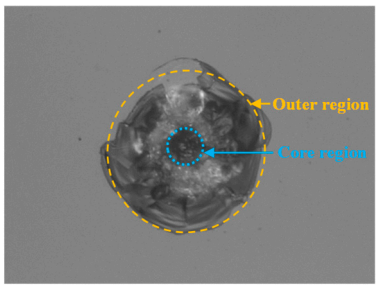

Figure 4. Optical microscopic image of a typical damage site on fused silica exit surface induced by a nanosecond pulse at 355 nm. The core region and the outer region of the damage site are indicated by blue and orange dashed circles, respectively.

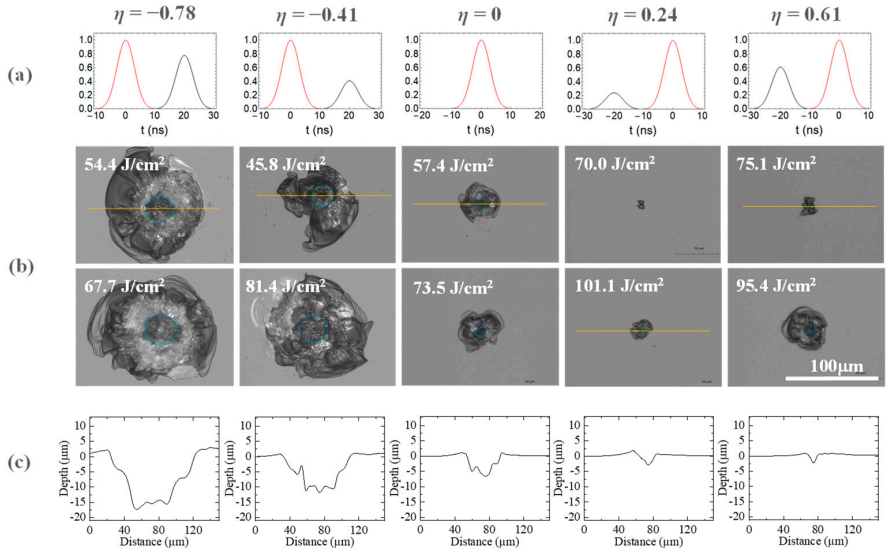

Figure 5. The representative damage morphology near threshold with different energy ratio η at the 20 ns delay. (**a**) The first row shows the dual-pulse train with various shape factors η. (**b**) The second and third rows shows the optical microscopic images of the damage sites while the applied fluence of main-pulse ϕ_{main} are marked in each image. All the images have the same scale. (**c**) The last row shows the line-out profile corresponding to the positions of the damage sites marked in orange. The sample surface is located at 0 μm on the vertical axis.

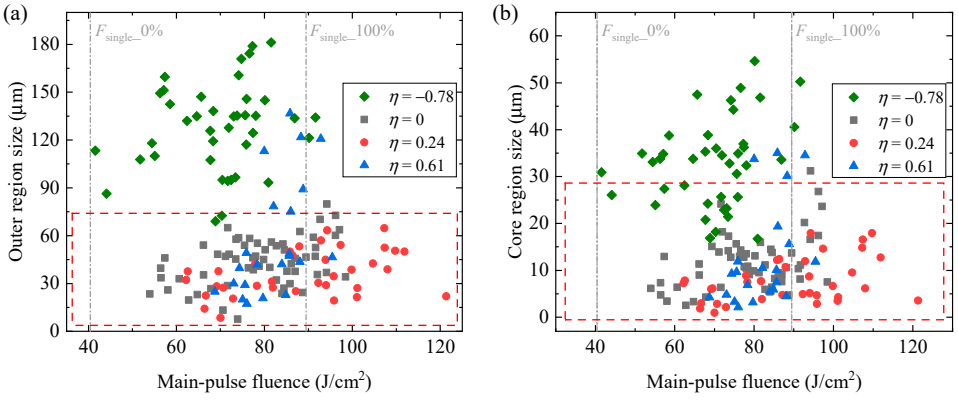

Figure 6. Size distributions of (**a**) the outer and (**b**) core regions of the damage sites on main-pulse fluence for $\eta = -0.78$, $\eta = 0$ (single-pulse), $\eta = 0.24$ and $\eta = 0.61$.

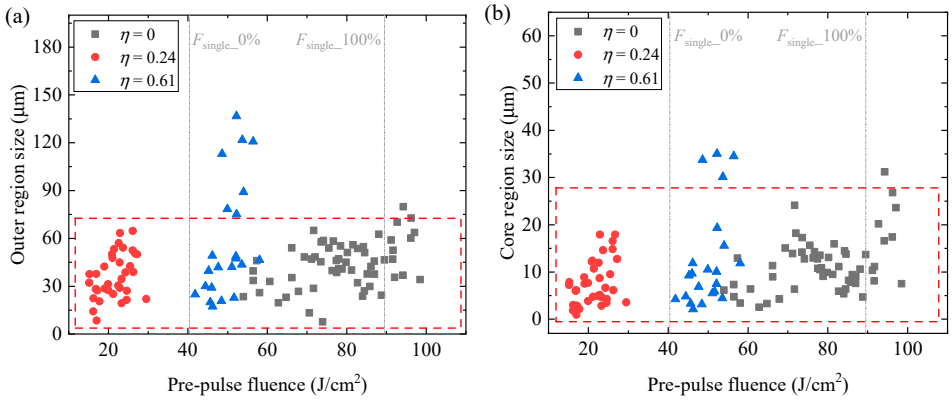

Figure 7. Size distributions of (**a**) the outer and (**b**) core regions of the damage sites on the pre-pulse fluence for η = 0 (single-pulse), η = 0.24 and η = 0.61.

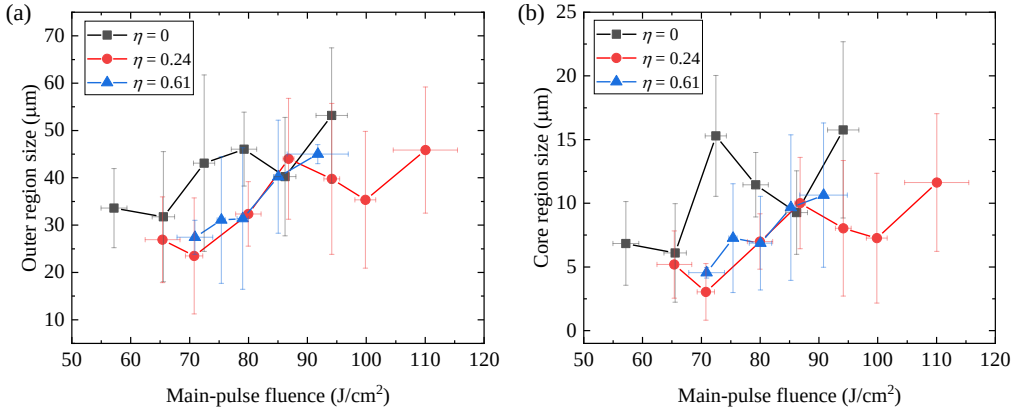

Figure 8. The statistical average size dependence of (**a**) the outer and (**b**) core regions of the damage sites on main-pulse fluence for η = 0 (single-pulse), η = 0.24 and η = 0.61 based the original data in the red dashed frames in Figure 6.

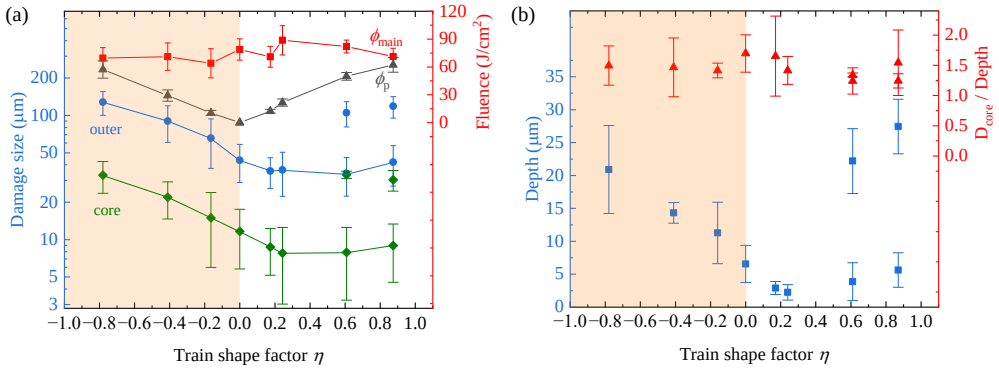

Figure 9. (**a**) Average damage size of the outer and core regions near the threshold as functions of the shape factor η at the 20 ns delay. The fluences for the main pulse and the pre- or post-pulse are also shown as the red squares and black triangles to reveal their roles in the modulation of the damage sizes. (**b**) Average damage depth (blue squares) and ratio of the core diameter to depth (red triangles) near the threshold as functions of the shape factor η at the 20 ns delay.

Although the damage sizes are discretely distributed in a certain range as shown in Figure 6, we present the representative damage sites at two stages of near-threshold fluence for various shapes factors in Figure 5. The single-pulse damage morphology (η = 0) is placed in the middle of Figure 5 as a comparison. In the last row of Figure 5, we give the corresponding line-out profile to provide the crater depth information of the damage sites

with the 3D digital microscope Hirox KH-8700. We can obtain that the temporal shape of dual-pulse train has great impacts on the morphology and size of the damage sites. First, the damage sites induced by the ramp-down shaped pulse-train are much larger and deeper than those by single pulse. Second, the damage sites induced by the ramp-up shaped pulse-train with η = 0.24 are significantly smaller and shallower than those by single pulse.

To reveal the exact effects of temporal shaping on the damage size, in Figure 6 we show the size distributions of the core and outer regions on the main-pulse fluence for representative shapes, i.e., η = −0.78, 0, 0.24 and 0.61. The data for the damage sizes are from the damage sites obtained in the damage threshold test in the fluence range of F_{main} ~2 F_{main}, the exact value of which varies for different shapes. The fluence range of F_{main} ~2 F_{main} is to ensure the reliability of the data statistics considering the probability of nanosecond damage. For η = −0.78, the size of the outer region ranges from 69.0 μm to 181.3 μm, while the size of the core region ranges from 16.7 μm to 54.6 μm. It can be seen that the damage sizes for the ramp-down shape with η = −0.78 are much larger than those for the three ramp-up shapes and single-pulse. For η = 0.61, however, when the main pulse fluence is larger than 80 J/cm^2, some damage sites are also very large and the sizes of the outer and core regions are up to 137 μm and 35 μm. To reveal the underlying cause, in Figure 7 we show the same size distributions of the core and outer regions on the pre-pulse fluence for the ramp-up shapes. For the shape factor η = 0.61, we can see that the fluences of the pre-pulse for all the damage sites are slightly larger than F_{single}, and especially those for the damage sites larger than 75 μm are larger than 1.25 F_{single}. Therefore, the pre-pulse for these sites is strong enough to excite the damage precursors and induce damage, and then the main pulse deposits a lot of energy in the damage core to result in a larger size of the final damage site, which is similar to the ramp-down shape case. In the following analysis and discussions, we distinguish these large damage sites from the damage sites with smaller sizes for the cases of η = 0.61 and η = 0.87 to focus on the modification effect of pre-pulse on the high-fluence precursors, rather than its effect on the damage initiation. To specifically analyze the reduction of the damage size by the ramp-up dual-pulse, based the original scatter data in the red dashed frames in Figure 6, we made a quantitative statistical analysis of the dependence of the average damage size on the main-pulse fluence for η = 0, η = 0.24 and η = 0.61 as shown in Figure 8. In terms of the statistical method, we combine the multiple data points in a narrow range of main-pulse fluence into one data point, and then obtain the mean value of the damage size with error bars. By comparing Figure 8a,b the size dependence on main-pulse fluence is similar for the outer and core regions and the damage size increases with the fluence. By comparing the three distribution curves of the average damage size with fluence for η = 0, 0.24, 0.61, the damage size at the same fluence for η = 0.24 is the smallest while that for η = 0 is the largest. Especially when the main-fluence is up to 110 J/cm^2 for η = 0.24, the damage size still remains in a low value. Although the dual-pulse shape for η = 0.61 has a higher threshold than that for η = 0.24, the sizes of the outer and core regions for η = 0.61 are slightly larger than those for η = 0.24. Therefore, by optimizing the ramp-up shape of dual-pulse, one can achieve higher damage thresholds and smaller average damage size at the same time, which has a great advantage in controlling the damage size in the high fluence regime.

In order to demonstrate directly the modulation law of temporal shaping on the damage size, we statistically calculated the average sizes of the damage sites with error bars for every shape factor and plot the curves of the average damage size with dual-pulse shape factor in Figure 9a. In term of the statistical method, we combined all the scatter data for a shape factor, such as those shown in Figure 6, into one value of the average size with the error bars of the damage size and laser fluence and thus obtained nine average damage sizes for nine shapes shown in Figure 9a. The right side of the vertical axis in Figure 9a indicates the average fluence of the main-pulse and pre- or post-pulse corresponding to the damage sites to reveal their role in the damage modulation. We can clearly see that the functions of the damage sizes of the outer and core regions on the shape factor are

significantly different between the two regimes of $\eta > 0$ and $\eta < 0$, i.e., the ramp-up and ramp-down shapes, respectively.

In the regime of $-0.78 \leq \eta < 0$, the pulse train has a ramp-down shape and it is the case of the post pulse. With the post-pulse fluence increasing from 0 to 57 J/cm^2 and the main-pulse fluence keeping almost constant, the average size of the outer region increases from 43.6 μm to 127.9 μm and that of the core region increases from 11.7 μm to 33.1 μm. The maximum of the average damage size at $\eta = -0.78$ is 127.9 μm, which is larger by 193% than that of single pulse. Since the main pulse can already induce laser damage, the post-pulse arriving after 20 ns is strongly absorbed by the resulted damage region by the main pulse. So the change of the post-pulse energy with the same main-pulse can precisely control the damage size by adjusting the absorbed energy.

In the regime of $0 < \eta \leq 0.87$, the pulse train has a ramp-up shape and it is the case of the pre-pulse. With gradually increasing the pre-pulse fluence from 0 to 62 J/cm^2, the average size of the outer region was reduced from 43.6 μm to 34.1μm while the size of the core region decreases from 11.7μm to 7.8μm. The size of the core region has a more obvious tendency to decrease relative to that of the outer region, and the core size for $\eta = 0.61$ is about 40% smaller than that for single-pulse. The core region is the zone for the energy absorption and deposition [25]. Therefore, the pre-pulse, smaller than single-pulse threshold, has a positive modification on the damage precursors and reduce the absorption ability so that the damage size after the dual pulse gets smaller than that of the single pulse. Thus the damage development was well suppressed at the sites effectively modulated by the pre-pulse. However, for some cases for $\eta = 0.61$ and 0.87, the dual-pulse meets the low fluence precursors, the pre-pulse already exceeds the damage threshold and causes the damage, and the main pulse energy is strongly absorbed by the pre-pulse damaged region, resulting a damage size of up to 105.5 μm. Therefore, there is an optimal pulse shape range for the modification effect of pre-pulse on the high-fluence precursors, while avoiding its effect on the damage initiation.

By comparing the two regimes of the ramp-up and ramp-down shapes, we can find that the temporal shaping has strong modulation on the sizes of the core and outer regions, and the average size of the outer contour can be continuously varied from ~130 μm to ~30 μm by adjusting the energy of post-pulse or pre-pulse. Therefore, temporal shaping can provide a valuable tool to produce the damage site with various sizes for the laser damage study, such as damage growth.

The effect of dual-pulse shape on the damage crater depth was also explored; see Figure 9b. We counted about five representative damage sites for each pulse shape. The curve trend of the crater depth with η is essentially the same as those of the damage sizes in Figure 9a, and the depth of the average core region decreases from ~22 μm to ~2.2 μm by increasing the factor η from -0.78 to 0.24. We further analyzed the ratio of the core diameter to the crater depth with η and found that the ratio was basically constant, i.e., ~1.5:1 in the range of 1.24:1 to 1.70:1. This indicates that the depth of the crater core is basically comparable to the radius, which is consistent with the single-pulse results presented in [26]. While the average size ratio of the outer region to the core is about 4.1:1 in the range of 3.7:1 to 4.7:1 at all the train shapes in Figure 9a, the ratio of the damage diameter to the crater depth was calculated to be about 6.2:1, which is consistent to the observations for the ratio of width to depth for pansies created at various pulse durations [26]. Therefore, the temporal shaping of the dual pulse does not change the depth–width ratio of the damage sites but significantly changes the damage size in a wide range. This indicates the same damage mechanism for the temporal shaped dual pulse as the single pulse, i.e., the inner molten core absorbs the majority of the laser energy while the outer region is mainly dominated by fractures. Therefore, modulation of temporal shaping on the damage size is realized by the control of the deposited energy in the core region.

3.3. Effect of Pulse Delay on Damage Threshold

As shown in Figure 3b, with the pre-pulse irradiation, the main pulse threshold is increased to exceed the single-pulse threshold and reach the maximum at the dual-pulse shape with η = 0.61. To investigate the temporal evolution of the pre-pulse effect on the precursor modification, we experimentally obtained the dependence of the main-pulse threshold on the pulse delay. We carried out damage threshold tests for the dual pulse with η = 0.61 by adjusting the pulse delay from 0 to 50 ns. The damage probability curves on the train fluence with different pulse delays were obtained by one-on-one tests; the results are shown in Figure 10a. Then, we calculated the main-pulse thresholds for 0% and 100% probability with the definition of η and show the dependences of main-pulse thresholds by pulse delay in Figure 10b. The inset in Figure 10b is the simulated dual-pulse shapes at delays of 0 ns, 5 ns, 10 ns and 20 ns, which show the exact temporal distributions of the pulse-trains.

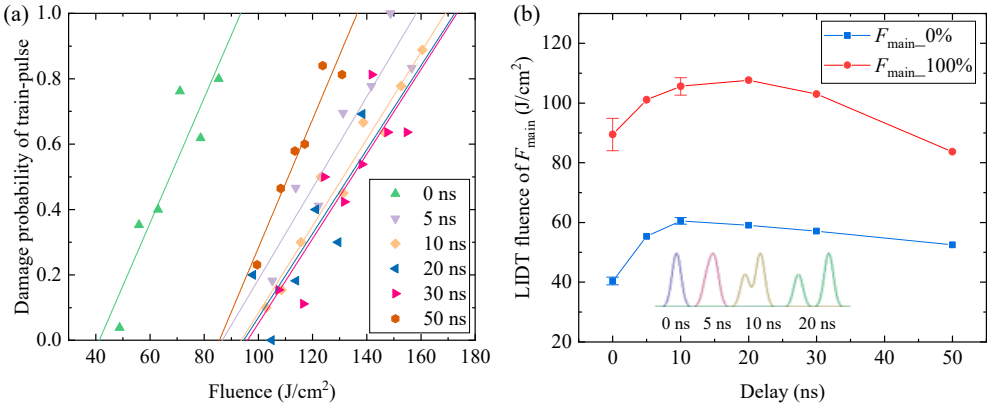

Figure 10. (**a**) Relations between damage probability and laser fluence of pulse train with various pulse delays for the shape factor η = 0.61. (**b**) Dependences of main-pulse threshold F_{main} (0% and 100% probability) on pulse delay. The inset is the sketches for the dual-pulse shapes at the delays of 0 ns, 5 ns, 10 ns and 20 ns.

For the 0% damage threshold, by increasing the pulse delay, the main-pulse threshold rapidly increases, reaching the maximum at 10 ns and then slowly decreasing. The threshold at a delay of 0 ns denotes the single-pulse threshold F_{single} of 40.4 J/cm^2, and the main-pulse threshold increases abruptly to 55.4 J/cm^2 at a 5 ns delay, where the FWHM width is about 10 ns. Although the threshold can be increased according to the scaling law of the damage threshold on the pulse width, the ramp-up shape also contributes to the larger threshold, as revealed by the pulse shaping of the 3 ns pulse on the damage threshold in [19]. The 0% threshold reaches the maximum of 60.5 J/cm^2 at a delay of 10 ns, where the peaks of the sub-pulse get separated in time, as shown in the inset of Figure 10b. When the delay is larger than 10 ns, the threshold slightly decreases, but the threshold at the 50 ns delay is still higher than that of the single-pulse threshold.

For the 100% damage threshold, the dependence of the main-pulse threshold on the pulse delay has the similar trend as that for the 0% threshold, but the maximum threshold is located at the delay of 20 ns. When the delay is 50 ns, the main-pulse threshold falls below single-pulse threshold. This means that the pre-pulse has a remarkable suppressing effect on the damage behavior of the main pulse with a delay of less than 50 ns.

4. Discussion

The experimental results prove the strong modulation of the damage threshold and morphology by temporal shaping of a dual pulse in the high fluence regime. In order to discuss and reveal the underlying physical mechanism, we propose a schematic diagram of the precursor modification and the damage initiation of fused silica exit surface by dual pulse with different temporal shapes, as shown in Figure 11.

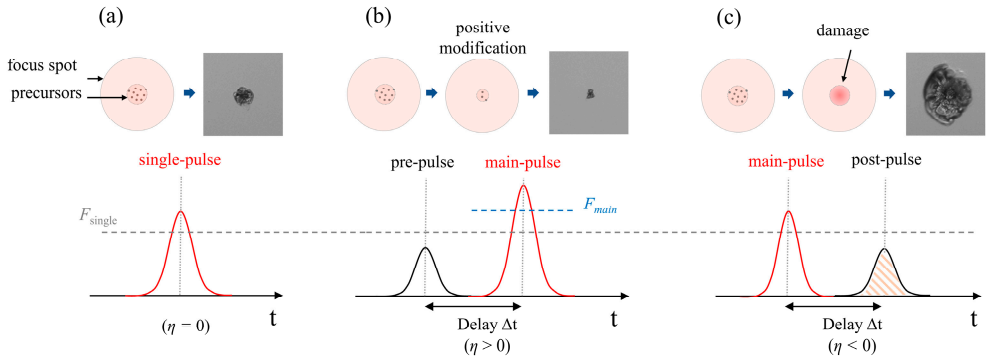

Figure 11. Schematic of a dual pulse acting on fused silica with temporal shaping. (**a**) Single pulse (η = 0); (**b**) the ramp-up shape with the pre-pulse (η > 0); (**c**) the ramp-down shape with the post-pulse (η > 0).

For the single pulse case with the Gaussian shape, i.e., η = 0, when the focal spot covers the damage precursors, the precursors will absorb the laser energy at the leading edge of the pulse, and the thermal diffusion generates the moving absorbing front, which will enhance the energy absorption by increasing the core area with high temperature [15,27,28]. The majority of energy deposited during laser-induced damage occurs in the laser-driven absorption front. This creates a molten core region in the damage site and a mechanically fractured outer region [10].

When η > 0, the pre-pulse with a low fluence produces a positive modification on the precursors, the optimal thermal melting could reduce the absorption ability to the subsequent laser irradiation [19,24,29], as shown in Figure 11b. As a result, the precursor becomes less susceptible to absorption when the main pulse irradiates on the same site, so the main pulse threshold is increased and once the damage is onset, the size of the damage sites is also slightly reduced. However, the exact modification mechanisms on damage precursors by the pre-pulse is still not clear and requires more efforts to explore. The experimental results show that, by applying the pre-pulse with a relatively low fluence, besides of higher main-pulse threshold, we can obtain the damage sites with smaller sizes than the single pulse, which will reduce the damage growth rate [30]. It could be useful and meaningful for the damage study in the high fluence regime.

While η < 0, the main pulse with high fluence can excite the precursors and produce an absorbing molten core [15,27,28]. When the subsequent post-pulse irradiated with the pulse delay is less than 50 ns, the absorbing front increases the area of the absorbing core; the temperature in the absorbing core is still thousands of degrees Kelvin [27,31], and the whole energy of the post pulse is well absorbed, which greatly increases the size of the damage sites [15,17]. The average damage size is monotonously dependent on the post-pulse energy, as shown in Figure 9a. Therefore, although the second pulse does not contribute to the damage initiation, by accurately choosing the post pulse energy, we can control the damage size by manipulating the deposited energy in the molten core region of the damage site.

Therefore, the sketched diagram of damage modulation by the dual pulse in Figure 11 can provides an instructive exploration on the damage dynamics control by temporal shaping of the pulse train. Such a modulation of the absorption dynamics can switch the modification of the precursors and the threshold improvement by pre-pulse to a worsening-damage process by the post-pulse.

5. Conclusions

In summary, the experimental results demonstrate that temporal shaping of a UV-nanosecond dual-pulse has an important influence on the damage threshold and morphology of a fused silica exit surface. For a pulse delay at 20 ns, the damage threshold and size were strongly modulated by changing shape factor η. The main-pulse damage threshold

was significantly improved by the pre-pulse due to a positive modification of the damage precursors, and when $\eta = 0.61$, F_{main} reached a maximum of 58.8 J/cm^2, which was 45.5% higher than F_{single}. Meanwhile, the average size of the damage site was slightly reduced by the pre-pulse. The post-pulse for $\eta < 0$ strongly deposited laser energy into the damage site initialized by the main pulse and eventually increased the damage size. The average size of the outer region gradually increased with an increase in the post-pulse fluence, reaching 127.9 μm at $\eta = -0.78$, i.e., 193% larger than that of a single pulse. At the condition of $\eta = 0.61$, the 0% damage threshold of the ramp-up dual-pulse increased with the delay and stabilized after 10 ns, while the 100% threshold reached the maximum at 20 ns. By temporal shaping of the dual-pulse train, one can switch the precursor modification by the pre-pulse to the absorption enhancement by the post-pulse. The presented results prove that temporal shaping of pulse trains is a valuable tool to study and manage damage dynamics, and the revealed physical mechanism could be helpful for a deeper understanding of the damage behavior in high fluence regimes.

Author Contributions: Conceptualization, M.S. and W.L.; methodology, M.S. and W.L.; validation, W.L., Y.G., Z.C. and Y.X.; formal analysis, M.S., Y.G. and W.L.; investigation, Y.S.; resources, J.Z. and M.S.; data curation, M.S. and W.L.; writing—original draft preparation, W.L.; writing—review and editing, M.S. and W.L.; supervision, M.S. and Z.J.; project administration, M.S.; funding acquisition, J.Z. and M.S. All authors have read and agreed to the published version of the manuscript.

Funding: This research was funded by National Natural Science Foundation of China, grant number 61975218; the "Strategic Priority Research Program" of Chinese Academy of Sciences, grant number XDA25020202 and Youth Innovation Promotion Association of the Chinese Academy of Sciences, grant number 2018282.

Institutional Review Board Statement: Not applicable.

Informed Consent Statement: Not applicable.

Data Availability Statement: The data that support the plots within this paper will be available from the corresponding authors upon reasonable request.

Conflicts of Interest: The authors declare no conflict of interest.

References

1. Manes, K.R.; Spaeth, M.L.; Adams, J.J.; Bowers, M.W.; Bude, J.D.; Carr, C.W.; Conder, A.D.; Cross, D.A.; Demos, S.G.; Nicola, J.M.G.D.; et al. Damage Mechanisms Avoided or Managed for NIF Large Optics. *Fusion Sci. Technol.* **2016**, *69*, 146–249. [CrossRef]
2. Jiao, Z.; Shao, P.; Zhao, D.; Wu, R.; Ji, L.; Wang, L.; Xia, L.; Liu, D.; Zhou, Y.; Ju, L.; et al. Design and performance of final optics assembly in SG-II Upgrade laser facility. *High Power Laser Sci. Eng.* **2018**, *6*, e14. [CrossRef]
3. Miller, P.E.; Bude, J.D.; Suratwala, T.I.; Shen, N.; Laurence, T.A.; Steele, W.A.; Menapace, J.; Feit, M.D.; Wong, L.L. Fracture-induced subbandgap absorption as a precursor to optical damage on fused silica surfaces. *Opt. Lett.* **2010**, *35*, 2702–2704. [CrossRef] [PubMed]
4. Suratwala, T.I.; Miller, P.E.; Bude, J.D.; Steele, W.A.; Shen, N.; Monticelli, M.V.; Feit, M.D.; Laurence, T.A.; Norton, M.A.; Carr, C.W.; et al. HF-Based Etching Processes for Improving Laser Damage Resistance of Fused Silica Optical Surfaces. *J. Am. Ceram. Soc.* **2011**, *94*, 416–428. [CrossRef]
5. Miller, P.E.; Suratwala, T.I.; Bude, J.D.; Laurence, T.A.; Shen, N.; Steele, W.A.; Feit, M.D.; Menapace, J.A.; Wong, L.L. Laser damage precursors in fused silica. In *Laser-Induced Damage in Optical Materials*; SPIE: Bellingham, WA, USA, 2009.
6. Neauport, J.; Lamaignere, L.; Bercegol, H.; Pilon, F.; Birolleau, J.C. Polishing-induced contamination of fused silica optics and laser induced damage density at 351 nm. *Opt. Express* **2005**, *13*, 10163–10171. [CrossRef]
7. Laurence, T.A.; Bude, J.D.; Ly, S.; Shen, N.; Feit, M.D. Extracting the distribution of laser damage precursors on fused silica surfaces for 351 nm, 3 ns laser pulses at high fluences (20–150 J/cm^2). *Opt. Express* **2012**, *20*, 11561–11573. [CrossRef]
8. Bude, J.; Miller, P.; Baxamusa, S.; Shen, N.; Laurence, T.; Steele, W.; Suratwala, T.; Wong, L.; Carr, W.; Cross, D.; et al. High fluence laser damage precursors and their mitigation in fused silica. *Opt. Express* **2014**, *22*, 5839–5851. [CrossRef]
9. Hu, G.; Zhao, Y.; Liu, X.; Li, D.; Xiao, Q.; Yi, K.; Shao, J. Combining wet etching and real-time damage event imaging to reveal the most dangerous laser damage initiator in fused silica. *Opt. Lett.* **2013**, *38*, 2632–2635. [CrossRef]
10. Wong, J.; Ferriera, J.L.; Lindsey, E.F.; Haupt, D.L.; Hutcheon, I.D.; Kinney, J.H. Morphology and microstructure in fused silica induced by high fluence ultraviolet 3ω (355 nm) laser pulses. *J. Non-Cryst. Solids* **2006**, *352*, 255–272. [CrossRef]
11. Carr, C.W.; Trenholme, J.B.; Spaeth, M.L. Effect of temporal pulse shape on optical damage. *Appl. Phys. Lett.* **2007**, *90*, 041110. [CrossRef]

12. Stuart, B.C.; Feit, M.D.; Rubenchik, A.M.; Shore, B.W.; Perry, M.D. Laser-Induced Damage in Dielectrics with Nanosecond to Subpicosecond Pulses. *Phys. Rev. Lett.* **1995**, *74*, 2248–2251. [CrossRef] [PubMed]
13. Carr, C.W.; Cross, D.A.; Norton, M.A.; Negres, R.A. The effect of laser pulse shape and duration on the size at which damage sites initiate and the implications to subsequent repair. *Opt. Express* **2011**, *19*, A859–A864. [CrossRef] [PubMed]
14. Laurence, T.A.; Negres, R.A.; Ly, S.; Shen, N.; Carr, C.W.; Alessi, D.A.; Rigatti, A.; Bude, J.D. Role of defects in laser-induced modifications of silica coatings and fused silica using picosecond pulses at 1053 nm: II. Scaling laws and the density of precursors. *Opt. Express* **2017**, *25*, 15381–15401. [CrossRef] [PubMed]
15. Carr, C.W.; Bude, J.D.; DeMange, P. Laser-supported solid-state absorption fronts in silica. *Phys. Rev. B* **2010**, *82*, 184304. [CrossRef]
16. Carr, C.W.; Cross, D.; Feit, M.D.; Bude, J.D. Using shaped pulses to probe energy deposition during laser-induced damage of SiO_2 surfaces. In *Laser-Induced Damage in Optical Materials*; SPIE: Bellingham, WA, USA, 2008.
17. Negres, R.A.; Feit, M.D.; DeMange, P.; Bude, J.D.; Demos, S.G. Pump and probe damage testing for investigation of transient material modifications associated with laser damage in optical materials. In *Laser-Induced Damage in Optical Materials*; SPIE: Bellingham, WA, USA, 2007.
18. Adams, J.; Weiland, T.; Stanley, J.; Sell, W.; Luthi, R.; Vickers, J.; Carr, C.; Feit, M.; Rubenchik, A.; Spaeth, M.; et al. *Pulse Length Dependence of Laser Conditioning and Bulk Damage in KD_2PO_4*; SPIE: Bellingham, WA, USA, 2005; Volume 5647.
19. Kafka, K.R.P.; Papernov, S.; Demos, S.G. Enhanced laser conditioning using temporally shaped pulses. *Opt. Lett.* **2018**, *43*, 1239–1242. [CrossRef]
20. Astrauskas, I.; Kaksis, E.; Flöry, T.; Andriukaitis, G.; Pugžlys, A.; Baltuška, A.; Ruppe, J.; Chen, S.; Galvanauskas, A.; Balčiūnas, T. High-energy pulse stacking via regenerative pulse-burst amplification. *Opt. Lett.* **2017**, *42*, 2201–2204. [CrossRef]
21. Li, M.; Menon, S.; Nibarger, J.P.; Gibson, G.N. Ultrafast Electron Dynamics in Femtosecond Optical Breakdown of Dielectrics. *Phys. Rev. Lett.* **1999**, *82*, 2394–2397. [CrossRef]
22. Nguyen, D.N.; Emmert, L.A.; Patel, D.; Menoni, C.S.; Rudolph, W. Transient phenomena in the dielectric breakdown of HfO_2 optical films probed by ultrafast laser pulse pairs. *Appl. Phys. Lett.* **2010**, *97*, 191909. [CrossRef]
23. Kafka, K.R.P.; Hoffman, B.N.; Kozlov, A.A.; Demos, S.G. Dynamics of electronic excitations involved in laser-induced damage in HfO_2 and SiO_2 films. *Opt. Lett.* **2021**, *46*, 1684–1687. [CrossRef]
24. Liu, W.; Sun, M.; Cui, Z.; Guo, Y.; Jiao, Z.; Wu, R.; Zhu, J. Modulation of laser damage by temporal shaping of double picosecond pulses. *Opt. Lett.* **2022**, *47*, 3856–3859. [CrossRef]
25. Demos, S.G.; Negres, R.A.; Raman, R.N.; Rubenchik, A.M.; Feit, M.D. Material response during nanosecond laser induced breakdown inside of the exit surface of fused silica. *Laser Photon. Rev.* **2013**, *7*, 444–452. [CrossRef]
26. Carr, C.W.; Matthews, M.J.; Bude, J.D.; Spaeth, M.L. The effect of laser pulse duration on laser-induced damage in KDP and SiO_2. In *Laser-Induced Damage in Optical Materials*; SPIE: Bellingham, WA, USA, 2006.
27. Carr, C.W.; Radousky, H.B.; Rubenchik, A.M.; Feit, M.D.; Demos, S.G. Localized Dynamics during Laser-Induced Damage in Optical Materials. *Phys. Rev. Lett.* **2004**, *92*, 087401. [CrossRef] [PubMed]
28. Grua, P.; Hébert, D.; Lamaignère, L.; Rullier, J.-L. Role of suprathermal electrons during nanosecond laser energy deposit in fused silica. *Appl. Phys. Lett.* **2014**, *105*, 081902. [CrossRef]
29. Michael, D.F.; Alexander, M.R. Implications of nanoabsorber initiators for damage probability curves, pulselength scaling, and laser conditioning. In *Laser-Induced Damage in Optical Materials*; SPIE: Bellingham, WA, USA, 2003.
30. Negres, R.A.; Abdulla, G.M.; Cross, D.A.; Liao, Z.M.; Carr, C.W. Probability of growth of small damage sites on the exit surface of fused silica optics. *Opt. Express* **2012**, *20*, 13030–13039. [CrossRef]
31. Demos, S.G.; Negres, R.A.; Raman, R.N.; Feit, M.D.; Manes, K.R.; Rubenchik, A.M. Relaxation dynamics of nanosecond laser superheated material in dielectrics. *Optica* **2015**, *2*, 765–772. [CrossRef]